Sepúlveda, FA.; Rivera, F.; Loyo, C.; Canales, D.; Moreno-Serna, V.; Benavente, R.; Rivas, LM.... (2022). Poly (lactic acid)/D-limonene/ZnO bio-nanocomposites with antimicrobial properties. Journal of Applied Polymer Science. 139(4):1-13. https://doi.org/10.1002/app.51542

F. A. Sepúlveda, F. Rivera, C. Loyo, D. Canales, V. Moreno-Serna, R. Benavente, L. M. Rivas, M. T. Ulloa, O. Gil-Castell, A. Ribes-Greus, J. A. Ortiz, P. A. Zapata. Poly(lactic acid)/D-limonene/ZnO bio-nanocomposites with antimicrobial properties. Journal of Applied Polymer Science, 2021; e51542

Poly(lactic acid)/D-limonene/ZnO Bio-Nanocomposites with Antimicrobial Properties

F. A. Sepúlveda [a], F. Rivera [a], C. Loyo [a], D. Canales [a], V. Moreno-Serna [a], R. Benavente [b], L. M. Rivas [c], M. T. Ulloa [c], O. Gil-Castell [d], A. Ribes-Greus [d], J. A. Ortiz [a,e], P. A. Zapata [a]*

Full text available at: https://onlinelibrary.wiley.com/doi/10.1002/app.51542

DOI: https://doi.org/10.1002/app.51542

Please, cite it as: F. A. Sepúlveda, F. Rivera, C. Loyo, D. Canales, V. Moreno-Serna, R. Benavente, L. M. Rivas, M. T. Ulloa, O. Gil-Castell, A. Ribes-Greus, J. A. Ortiz, P. A. Zapata. Poly(lactic acid)/D-limonene/ZnO bio-nanocomposites with antimicrobial properties. Journal of Applied Polymer Science, 2021; e51542

a. Universidad de Santiago de Chile (USACH), Facultad de Química y Biología, Departamento de Ciencias del Ambiente, Grupo Polímeros, Chile. (paula.zapata@usach.cl).
b. Instituto de Ciencia y Tecnología de Polímeros, ICTP-CSIC, Juan de la Cierva, 3. 28006 Madrid, Spain.
c. Programa de Microbiología y Micología, ICBM-Facultad de Medicina Universidad de Chile, dirección, Avenida Independencia 1027, Comuna Independencia, Santiago, Chile.
d. Instituto de Tecnología de Materiales (ITM), Universitat Politècnica de València (UPV), Camino de Vera S/n, 46022, Valencia, Spain.
e. Departamento de Ingeniería Química, Biotecnología y Materiales, Facultad de Ciencias Físicas y Matemáticas, Universidad de Chile, Avenida Beaucheff 851, Santiago, Chile.

*Corresponding author: paula.zapata@usach.cl

F. A. Sepúlveda, F. Rivera, C. Loyo, D. Canales, V. Moreno-Serna, R. Benavente, L. M. Rivas, M. T. Ulloa, O. Gil-Castell, A. Ribes-Greus, J. A. Ortiz, P. A. Zapata. Poly(lactic acid)/D-limonene/ZnO bio-nanocomposites with antimicrobial properties. Journal of Applied Polymer Science, 2021; e51542

Poly(lactic acid)/D-limonene/ZnO Bio-Nanocomposites with Antimicrobial Properties

F. A. Sepúlveda [a], F. Rivera [a], C. Loyo [a], D. Canales [a], V. Moreno-Serna [a], R. Benavente [b], L. M. Rivas [c], M. T. Ulloa [c], O. Gil-Castell [d], A. Ribes-Greus [d], J. A. Ortiz [a,e], P. A. Zapata [a]*

Abstract

Antimicrobial films of PLA/D-limonene/ZnO-based bio-nanocomposites were prepared via melt compounding and subsequent thermocompression. ZnO pure nanoparticles and organically modified with oleic acid (O-ZnO), with an average diameter of 13.5 nm, were incorporated at concentrations of 3, 5, and 8 wt% into polymer. D-limonene acted as a plasticizer was also incorporated at concentrations of 10 or 20 wt% into the PLA, given the decrease in the glass transition temperature compared to pure PLA. The presence of ZnO and O-ZnO in the PLA matrix promoted a slight increase in the degree of crystallinity (X_c) due to its nucleant performance. Although ZnO and O-ZnO induced lower thermal stability and slightly decreased microhardness in the composites, excellent antimicrobial performance was demonstrated. Both ZnO and O-ZnO nanocomposites reached 99.9% of effectiveness for nanoparticles content above 5 wt%, regardless of the source of irradiation, D-limonene concentration, and nanoparticle modification. These bio-nanocomposites will allow for future advances in sustainable antimicrobial materials for the medical or food packaging fields.

Keywords

polylactide (PLA), D-limonene, zinc oxide (ZnO), bio-nanocomposites, antimicrobial

1. Introduction

Poly (lactic acid) (PLA) is one of the most promising polymers due to its renewable origin and biodegradability, which would reduce the effects of the carbon footprint and allow for sustainable waste disposal strategies [1,2]. PLA is a derivate of lactic acid obtained from renewable resources such as corn, beets, and wheat. It is industrially obtained using thermophile bacteria by fermentation or ring-opening polymerization (ROP) of the lactide monomer. [3,4]

PLA is considered a feasible alternative for replacing petrochemical polymers [4,5], due to its unique features such as transparency, mechanical properties, low toxicity, low cost, and controlled biodegradability. [6,7] Indeed, it offers high potential and advantages in a range of industrial applications, such as packaging or medical device fabrication. [8–10] However, the intrinsic chain rigidity may become a disadvantage, given the low chain mobility, which may result in low tensile elongation at break and low toughness, limiting its applicability in its pure state. In this regard, plasticizers are commonly used in PLA to enhance chain mobility and also facilitate processability. [11–14]

D-limonene is a natural compound from the family of terpenes that can be found in the oil of citrus fruit peel. [13] Previous works reported the use of D-limonene as a plasticizer for PLA due to its good miscibility [15], leading to an increase in the tensile strain behavior, lower elastic modulus, and lower glass transition temperature. [15,16] Up to 20 wt% D-limonene has been proved miscible with PLA, and has been successfully used to plasticize PLA by conventional extrusion.[16] Moreover, D-limonene's antibacterial and antifungal power has been reported to inhibit the growth of a wide range of bacteria and fungi. [17,18]

With the aim of growth and reducing microorganisms' adhesion in the PLA, nanoparticles such as silver, copper, or photoactive oxides, such as TiO_2 with antimicrobial activity, are usually considered feasible alternatives. [3,19–21] Nevertheless, the toxicity of silver nanoparticles is still under evaluation, and titanium dioxide (TiO_2) requires the use of UV irradiations for activation. [22] Alternatively, zinc oxide (ZnO) nanoparticles are of great interest as antimicrobial compounds, as they are non-toxic to the human body, economically affordable, easy to synthesize, and are highly stable at elevated temperatures. [3,23] ZnO is generally recognized as a safe (GRAS) material by the Food and Drug Administration (FDA) and is sometimes used as a food additive. [24] Indeed, ZnO has shown antimicrobial activity against a broad spectrum of microorganisms such as *E. coli, Pseudomonas aeruginosa,* and *Staphylococcus.* [23,25] In an aqueous solution under UV radiation, the ZnO nanoparticles produce reactive oxygen species (ROS), such as hydrogen peroxide (H_2O_2) and superoxide ions (O_2^-), which have phototoxic effects on these microorganisms. Thus, these ROS are capable of inhibiting or killing bacteria by penetrating their membranes. [26] Complementarily, the release of zinc ions (Zn^{2+}) has been proposed as an antibacterial mechanism for the ZnO nanoparticles, affecting transport processes, amino acid metabolism, and enzyme system disruption. [27,28]

PLA with antibacterial properties by the addition of ZnO nanoparticles has been reported for textile, packaging, and medicinal applications [29,30], and different methods are applied: (*i*) Biocidal PLA/ZnO packaging films (ZnO with cubic morphology, 56 nm, 0-1.5 wt%) obtained by solution casting revealed stronger antimicrobial activity against Gram-negative bacterium *E. coli* than a Gram-positive one (*Listeria monocytogenes).* [31] Moreover, in the composites, tensile strength increased by 37.5%, and water vapor permeability (WVP) decreased by 30.5% compared to pure PLA. (*ii*) PLA/ZnO composites prepared with functionalized rod-like ZnO nanoparticles were active against *S. aureus and E. coli*. However, the use of untreated ZnO nanoparticles was demonstrated to produce severe degradation of the PLA during melt processing, ascribed to the transesterification reactions of the matrix. [6] (*iii*) PLA/ZnO nanocomposite films further showed excellent antimicrobial properties against *S. aureus* and *Klebsiella pneumoniae*. Although the mechanical properties of the nanocomposites may be compromised, the surface treatment of nanofillers by silanization [32] or organosilananization [33] limited the molar mass decrease of the PLA and allowed for better dispersion of the nanoparticles, thus increasing antimicrobial performance. (*iv*) PLA nanocomposites with Cu-doped ZnO nanoparticles (0-1.5 wt%) functionalized with Ag nanoparticles, using o-acetyl citrate/Lapol 108 as plasticizer, were obtained by melt mixing and were found to inhibit the growth of *P. aeruginosa*. [24] However, they were not efficient as antimicrobial packaging against *S. aureus*. The use of plasticizers resulted in greater elongation at break, lower tensile strength at break, and elastic modulus. Complementarily, the degree of crystallinity of the nanocomposites increased with the nanoparticle content. (*v*) Multifunctional active PLA/ZnO films with nanometric ZnO particles (2-20 nm) deposited in natural aluminosilicates with hollow, cylindrical-shaped nanotubes (HALs) (2.5-10 wt%) have been prepared by solution casting. [1] Although these functional materials showed significant antimicrobial properties, they had higher rigidity and lower elongation at break than the neat PLA, which may hinder its applicability in packaging films that require high ductility. In this regard, the addition of a plasticizer into ZnO-HAL/PLA nanocomposites was reported as a suitable option to improve the flexibility of the nanocomposite films.

Therefore, based on previous works of PLA matrices with the addition of D-limonene as a plasticizing agent would allow obtaining a polymer composite with more flexibility than neat PLA. On the other hand, the organic functionalization of ZnO nanoparticles with oleic acid would provide better compatibility and distribution of the nanoparticles into polymeric matrix. These findings show that ZnO nanoparticles are an excellent alternative as an antimicrobial filler in polymer nanocomposites to be applied for food packaging with appropriate mechanical properties.

Altogether, this research pursues the preparation of antimicrobial films of PLA/ZnO nanocomposites via melt compounding and subsequent thermocompression, containing D-limonene as a plasticizer. The ZnO nanoparticles with an average diameter of 13.5 nm were obtained by the sol-gel method, superficially and organically modified with oleic acid (O-ZnO). The effect of the D-limonene in the blends and the different amounts of ZnO and O-ZnO (5 and 8 wt%) on the thermal and mechanical properties were evaluated. Finally, the antimicrobial behavior of the PLA/D-limonene, PLA/D-limonene/ZnO, and PLA/D-limonene/O-ZnO was demonstrated against *E. coli,* maintaining suitable properties use in the preparation of films for packaging.

2. Materials and methods

2.1. Materials and reagents

Poly(lactic acid) (PLA) was purchased from Oxiquim as PLA pellets with a density of 1.24 g/cm^3, molecular mass of 73.500 g/mol, and with a PDLA stereoregularity. [34] For the synthesis of the nanoparticles, sodium hydroxide (Merck KGaA, reagent grade, 99%), zinc chloride (Merck, reagent grade 80–100%), distilled water, and 2-propanol (Equilab, reagent grade 99.8%) were used. The reagents used for organic nanoparticle modifications were oleic acid (Sigma-Aldrich, 90%) and hexane as solvent (J.T.Baker 99.8%), and D-limonene (Aldrich, reagent grade 97%) was used as plasticizer.

2.2 Synthesis of ZnO nanoparticles

The ZnO nanoparticles were obtained by the sol–gel method reported previously. [32–34] The precursor solution was obtained by adding 5.5 g of $ZnCl_2$ to 200 mL of distilled water (0.2 M) at

90 ºC in an oil bath. The second solution was prepared with 5 M NaOH in distilled water, and it was added dropwise to the first solution, stirring during 10 min at 90 ºC. The suspension was washed with distilled water to reduce the NaCl concentration below 10^{-6} M, as verified with a silver nitrate ($AgNO_3$) solution. The particles were mixed with 2-propanol in an ultrasonic bath during 10 min at 20 ºC. Next, the particles were centrifuged at 5000 RPM during 15 min, and they were then washed three times with 2-propanol at 60 ºC. Finally, the particles were calcined at 250 ºC during 5 h in order to obtain ZnO.

2.3 Organic modification of ZnO nanoparticles

The organic modification method to obtain O-ZnO was previously described. [23,35–37] First, 1-Hexane (100 mL) and oleic acid (200 μL) were mixed with stirring. Then 1 g of ZnO nanoparticles were added to the solution at 60 ºC with vigorous stirring for 5 h. Finally, the nanoparticles were filtered, washed with ethanol, and vacuum-dried at 100 °C during 24 h.

2.4. Preparation of the nanocomposites

The nanocomposites contained different concentrations of ZnO or O-ZnO nanoparticles (3, 5, and 8 wt%) and D-limonene (10 or 20 wt%) as a plasticizer. The PLA was previously dried at 90 ºC for 6 h before the melting process. The preparation of neat PLA, PLA/D-limonene, PLA/D-limonene/ZnO, and PLA/D-limonene/O-ZnO nanocomposites were carried out in a Brabender Plasticorder in an inert atmosphere (N_2) at 190 ºC, with a mixing speed of 110 rpm for 10 min. Afterwards, the samples were press molded at 190 ºC at 50 bar for 5 min in a LabTech Engineering Scientific hydraulic press and cooled under pressure by flushing the press with cold water. The dimensions of the films were 12×12 cm and 0.1 cm in thickness. **Table 1** gathers the composition and designation of the obtained blends and nanocomposites.

Table 1. Composition and designation of the obtained blends and nanocomposites.

D-limonene (wt%)	ZnO (wt%)	O-ZnO (wt%)	Designation
-	-	-	PLA
10	-	-	PLA/DL10
	3	-	PLA/DL10/ZnO3
	5	-	PLA/DL10/ZnO5
	8	-	PLA/DL10/ZnO8
	-	3	PLA/DL10/O-ZnO3
	-	5	PLA/DL10/O-ZnO5
	-	8	PLA/DL10/O-ZnO8
20	-	-	PLA/DL20
	3	-	PLA/DL20/ZnO3
	5	-	PLA/DL20/ZnO5
	8	-	PLA/DL20/ZnO8
	-	3	PLA/DL20/O-ZnO3
	-	5	PLA/DL20/O-ZnO5
	-	8	PLA/DL20/O-ZnO8

2.4. Physical-chemical characterization of nanoparticles and nanocomposites

The morphology of the ZnO nanoparticles and their dispersion in the composites was analyzed by TEM (Philips, model Tecnai 12) operating at 20 kV. Samples for TEM measurements of nanoparticles were prepared by placing a drop of ZnO previously mixed with ethanol and sonicated on a carbon-coated standard copper grid (400 mesh) and evaporating the ethanol used as a solvent. For the nanocomposites, ultra-thin specimens with a thickness of ca. 200 nm were cut with glass blades. To determine the diameter of the nanoparticles, the images obtained were processed using the ImageJ 1.49q software.

The crystalline structures of the ZnO and O-ZnO nanoparticles was assessed employing X-Ray diffraction (XRD). Spectrums were obtained using a Siemens D5000 diffractometer using Ni-filtered Cu Kα radiation (λ = 0.154 nm).

The chemical structure of the ZnO and O-ZnO nanoparticles was analyzed by Fourier transform infrared (FTIR) in a Bruker Vector 22 FTIR spectrometer. The FTIR analysis was permormed by preparing pellets of the samples with KBr. The IR spectra were collected in the 4000 to 500 cm^{-1} range at room temperature with a resolution of 4 cm^{-1} and an accumulation of 64 scans.

The thermal properties of the neat PLA, PLA/D-limonene, PLA/D-limonene/ZnO, and PLA/D-limonene/O-ZnO nanocomposites were measured by differential scanning calorimetry (DSC) using a Mettler-Toledo DSC822^e device. The samples were heated from 25 to 180 ºC at a rate of 10 ºC/min, and then cooled to 25 ºC at the same rate; the values were taken from the second heating curve to eliminate any thermal history. The degree of crystallinity (X_c) was calculated using **Equation (1)**.

$$X_c(\%) = \frac{(\Delta H_m - \Delta H_{cc})}{\Delta H_m{}^0 (f_{PLA})} \times 100 \qquad (\mathbf{1})$$

where ΔH^o_m is the enthalpy of fusion of an ideal 100% crystalline PLA (93 $J \cdot g^{-1}$) [3,38], ΔH_m and ΔH_{cc} are the melting and cold crystallization enthalpies, respectively, and f_{PLA} is the effective weight fraction of PLA. [16]

In order to characterize the crystalline structure in depth, the lamellar thicknesses were calculated applying the Thomson-Gibbs equation (**Equation (2)**), based on the temperatures associated with the melting transitions [39,40],

$$l_C(T_m) = \left[\left(1 - \frac{T_m}{T_m^0}\right) \cdot \frac{\Delta h_{mV}}{2 \cdot \sigma_e}\right]^{-1} \qquad (\mathbf{2})$$

where T_m is the melting peak temperature; $T_m{}^0$ is the equilibrium melting temperature of an infinite crystal (480 K); σ_e is the surface free energy of the basal plane where the chains fold ($60.89 \cdot 10^{-3}$ J·m^{-2}); and Δh_{mV} is the melting enthalpy per volume unit ($111.083 \cdot 10^{8}$ J·m^{-3}). [41]

The thermal stability was evaluated through thermogravimetric analysis (TGA) using a TGA/SDTA 851 Mettler-Toledo setup under Argon inert atmosphere (50 mL·min^{-1}). Samples in triplicates were introduced into alumina crucibles and heated from 25 ° C to 600 ° C at a heating rate of 10 ºC·min^{-1}.

The microhardness of the neat PLA and the nanocomposites were measured in a Vickers hardness (*HV*) Leitz Miniload 2 setup at 29 ºC under a charge of 0.981 N during 25 s. *HV* values were calculated in MPa according to **Equation (3)**. [42]

$$HV = 2\sin 68\left(\frac{P}{D^2}\right) \qquad \mathbf{(3)}$$

where *P* is the contact load in N and *D* is the diagonal length of the projected indentation area in mm.

The antimicrobial effect of the different samples was determined using a plate count method described in the ISO 20743. [43] *E. coli* ATCCC 25922 was used as microbes for analysis. In brief, the initial number of bacteria present after incubation was calculated by counting the number of colonies in a ten-fold dilution. Starting from a fresh culture, a microbial suspension of $1 \cdot 10^{7}$ CFU·mL^{-1} by densimat bioMérieux® was prepared in a BHI broth plus Triton 100x in a humid chamber. 0.5 mL of the suspension was placed in contact with every 2.5 cm^{2} sample. Control and antibacterial-treated samples were recovered by suspension in 10 mL of sterile saline solution and then serially diluted down to 1/10, 1/100, and 1/1000. Then, 0.2 mL of each dilution in duplicate was plated on trypticase soy agar plates and incubated at 37 ºC for 24 h under UV and white light. After incubation, the number of colonies in the Petri dishes were counted, and the percentage of inhibition was determined in comparison to its corresponding control. The percentage of colony reduction was calculated using **Equation (4)**, which relates the number of colonies of the neat polymer to the number of colonies from the nanocomposites.

$$Reduction\ (\%) = \frac{CFU\ neat\ Polymer - CFU\ nanocomposite}{CFU\ neat\ Polymer} \times\ 100 \qquad \mathbf{(4)}$$

3. Results and discussion

3.1. Nanoparticles characterization

The nanoparticle morphology was studied by transmission electron microscopy (TEM). **Figure 1** displays the TEM images and the obtained diameter histogram of ZnO nanoparticles. In general, irregular spherical shapes with an average diameter of 13.5 nm were found.

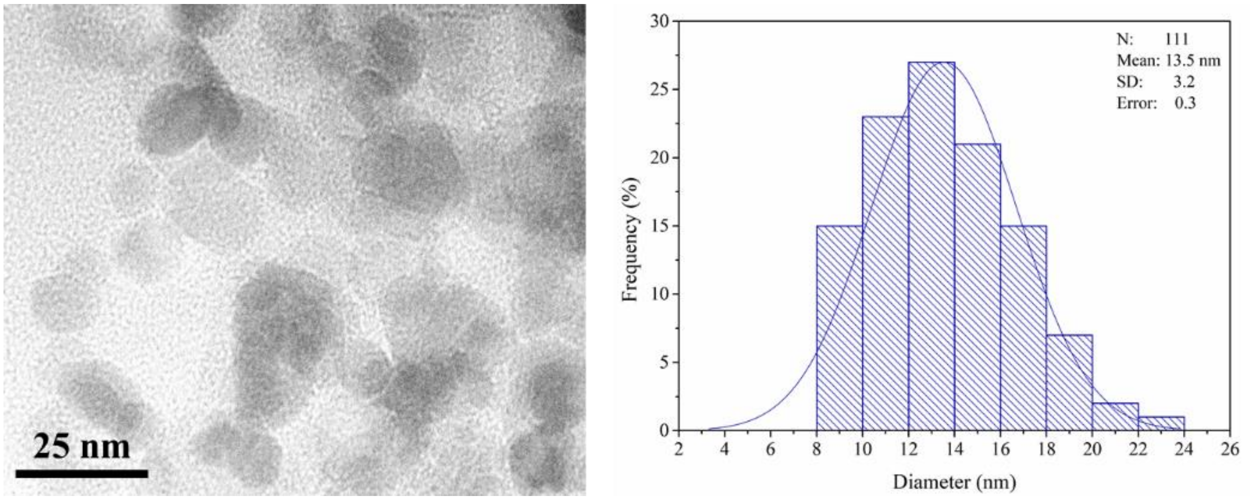

Figure 1. TEM images and histogram of ZnO nanoparticles.

The crystalline structure of the ZnO and O-ZnO nanoparticles were verified by X-ray diffraction (XRD), as shown in **Figure 2**. The diffractogram of both nanoparticles showed Bragg's reflection at 2θ = 32, 34, 36, 47, 56, 63, 66, 68, 69, 72 and 77°, corresponding to the (100), (002), (101), (102), (110), (103), (200), (112), (201), (004), and (202) crystal planes characteristic of the wurtzite phase of ZnO. [44,45] The crystalline structure of the O-ZnO nanoparticles remained unaltered after organic modification. The highest peak at 2θ = 36° corresponds to plane (101), corroborated by other authors. [31,44] The diffractograms only showed the peaks associated with the crystalline structure of ZnO, therefore demonstrating the purity of the obtained nanoparticles.

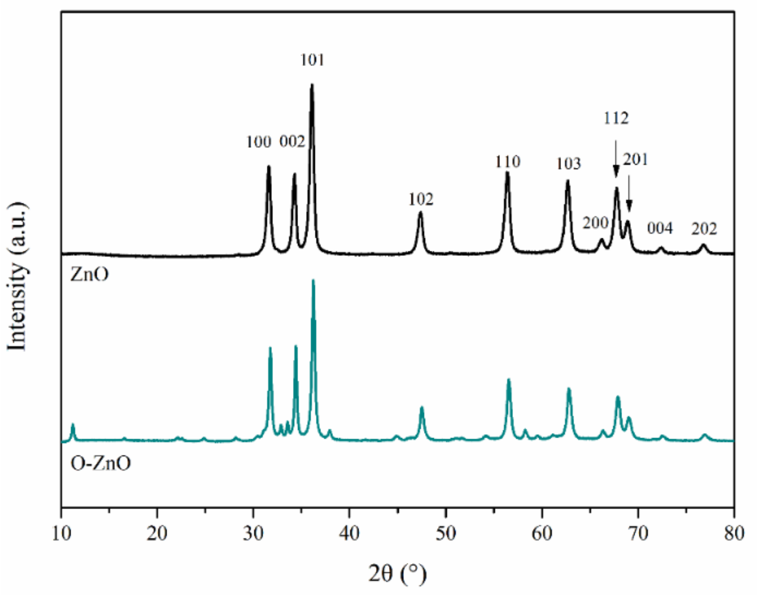

Figure 2. XRD diffractograms of ZnO and O-ZnO nanoparticles.

The infrared spectrum of ZnO, oleic acid, and O-ZnO are shown in **Figure 3**. The ZnO nanoparticles showed the characteristic broadband at 3600-3100 cm^{-1} associated with the O-H stretching of hydroxyl groups on the ZnO surface and the low-intensity band at 1585 cm^{-1}, attributed to the O-H flexion vibration mode of the humidity retained in the samples. [44] In the fingerprint region of ZnO nanoparticles, two signals at 980-670 cm^{-1} are assigned to stretching and deformation vibration modes of the Zn-O bond. The spectrum of oleic acid shows a broadband at ~3000 cm^{-1} attributed to the O-H stretching of the carboxylic acid dimer. In the 2930-2850 cm^{-1} region, signals were assigned to symmetric and asymmetric aliphatic C-H stretching vibrations of the oleic acid backbone. The strong band at 1712 cm^{-1} was assigned to asymmetric stretching of C=O of the saturated carboxylic acid. [46,47] The weak band at 1460 cm^{-1}

corresponds to the bending of C-OH. Furthermore, it presents other weak bands at 1400 and 1290 cm^{-1} attributed to bending of -CH_2- from the oleic acid aliphatic chain.

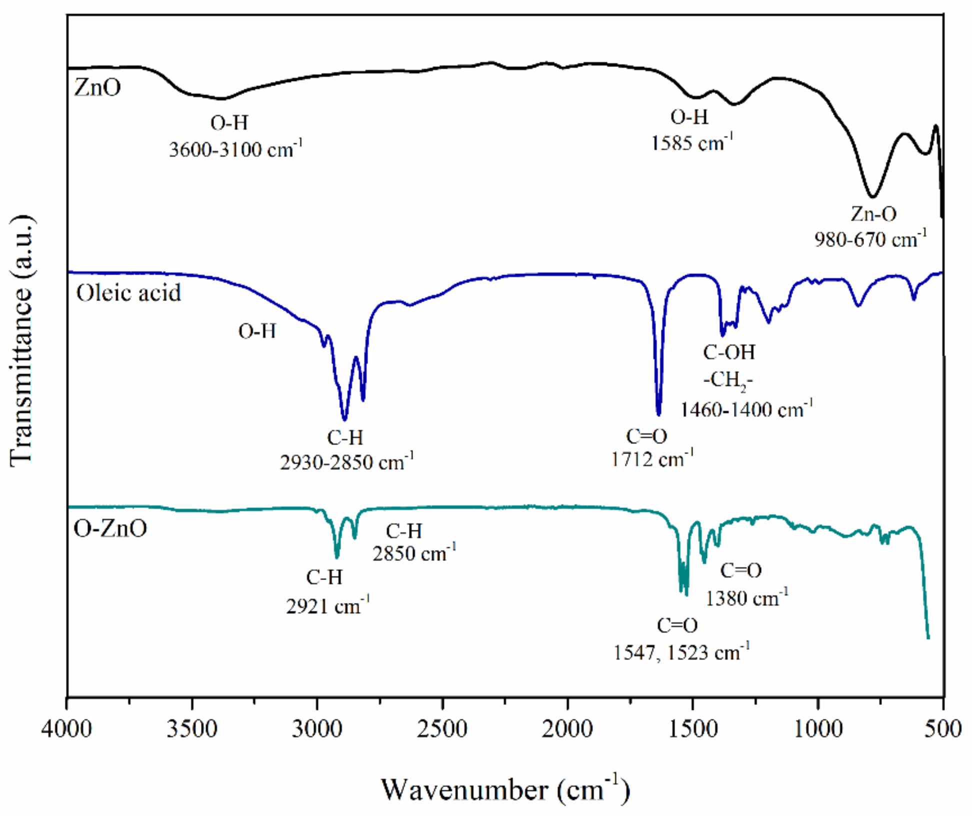

Figure 3. FT-IR spectra of ZnO nanoparticles, oleic acid, and O-ZnO nanoparticles.

The O-ZnO spectrum exhibited new bands compared to neat ZnO nanoparticles at 2850 and 2921 cm^{-1} related to symmetric and asymmetric aliphatic C-H stretching vibrations. New bands ~~at 1547 (C=O), 1523 (C=O), and 1380 cm^{-1} (C=O)~~ between 1547-1380 cm^{-1} appeared due to the carboxylate group, associated with the reaction between the carboxylic acid group from the fatty acid oleic acid and the hydroxyl groups from the surface of ZnO nanoparticles. [35,44] This reaction involves an acid-base reaction between the carboxylic acid and the dibasic $Zn(OH)_2$, forming the zinc oleate salt. It is constituted by carboxylate and Zn^{2+} ions. The carbon-oxygen bond order in the carboxylate groups is about 1.5 (average between C=O and C-O bonds), and thus the classical carboxylic acid C=O stretching wavenumber is shifted to lower values. The carboxylate groups exhibit a high-intensity doublet at 1547 and 1523 cm^{-1} and a signal at 1380 cm^{-1} assigned to the asymmetric and symmetric stretching vibration modes, respectively. [48,49] The intensity of these bands is related to the high dipole moment of the C-O bonds. The weak band at 1450 cm^{-1} is assigned to the bending of $-CH_2-$ groups from the zinc oleate aliphatic chain. [49] Moreover, a tiny band at 1733 cm^{-1} could be attributed to the saturated ester C=O stretching produced by the esterification reaction of oleic acid with the superficial $Zn(OH)_2$ of the ZnO nanoparticles. Therefore, these results verify the successful organic chemical modification of ZnO nanoparticles with oleic acid.

3.2. Nanoparticle dispersion in the composites

The distribution of the ZnO and O-ZnO into the nanocomposites was studied by transmission electron microscopy (TEM). For representative purposes, the obtained electron micrographs for the nanocomposites of PLA with D-limonene (10 wt%) and nanoparticles (5 wt%) are shown in **Figure 4**. The surface modification of ZnO nanoparticles with oleic acid improved the dispersion of the nanoparticles into PLA, which leads to enhance compatibility and an increased in the interaction between nanoparticles and polymer. Similar results had been reported to use oleic acid as organic modifier of the different nanoparticles in order to improved in the nanoparticles dispersion into the polymer. [23,35,36,50] The D-limonene was used in this study in order to improve the PLA and nanocomposites processibility by extrusion method. [15,51,52] In general, it is observed that the O-ZnO nanoparticles were uniformly dispersed into the PLA matrix, showing that the incorporation of D-limonene is effective in obtaining suitable nanocomposites.

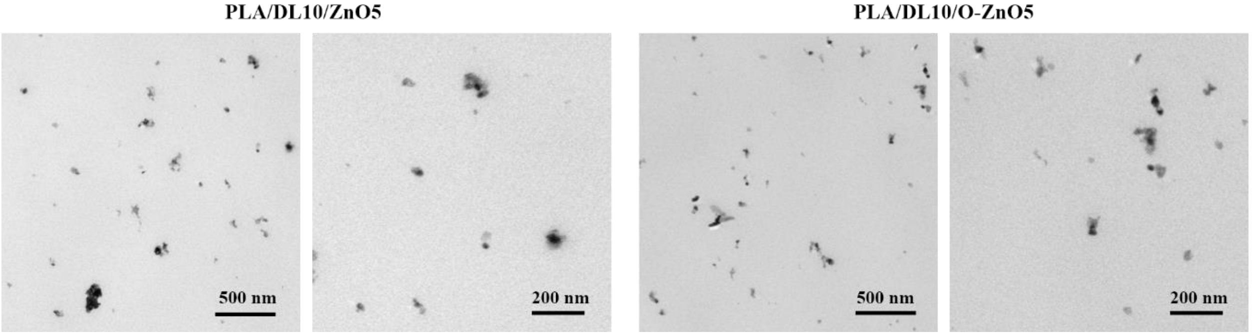

Figure 4. TEM images of PLA nanocomposites with D-limonene (10 wt%) and ZnO (5 wt%) (left), and O-ZnO (5 wt%) (right).

3.3. Thermal properties

The thermal properties were assessed using differential scanning calorimetry (DSC). The obtained thermograms for pure PLA, plasticized PLA, nanocomposites with D-limonene (10 and 20 wt%), and nanoparticles (3 wt%) are shown in **Figure 5**. The obtained thermograms for all compositions were further characterized in terms of peak temperatures of the described transitions, and results are gathered in **Table 2**. Particularly, the glass transition temperature (T_g), cold crystallization temperature (T_{cc}), and melting temperature (T_m) were assessed. Moreover, the crystallinity degree (X_c) of the neat PLA, PLA/D-limonene, and PLA/D-limonene/ZnO and PLA/D-limonene/O-ZnO nanocomposites was calculated.

As expected for semicrystalline PLA, the curves revealed three thermal transitions. First, an endothermic peak was associated to structural relaxation during the glass transition. Then, an exothermic transition was found, due to the cold crystallization process. Finally, a melting process for the crystalline domains was found. The appearance of a cold crystallization and subsequent melting peak with a comparable enthalpy denotes the low crystalline character of the samples after processing. [53]

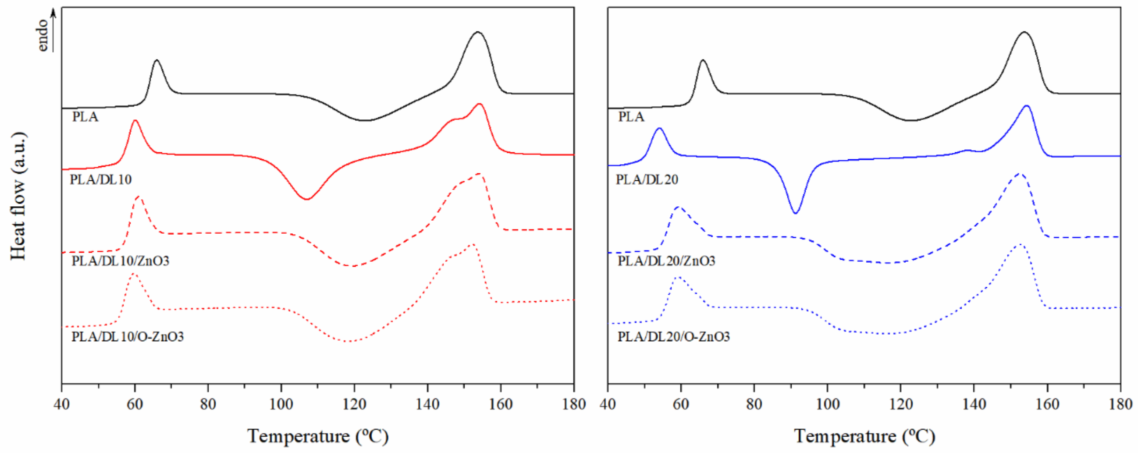

Figure 5. DSC thermograms of neat PLA, PLA/D-limonene, and nanocomposites with D-limonene (10 wt%, left; and 20wt%, right).

Table 2. Results of the thermal properties for neat PLA, PLA/D-limonene, and nanocomposites. Standard deviation between 1 and 2% was omitted for the sake of clarity.

	T_g (ºC)	**T_{cc} (ºC)**	**T_{m1} (ºC)**	**T_{m2} (ºC)**	**l_{c1} (nm)**	**l_{c2} (nm)**	**ΔH_m (J/g)**	**X_c (%)**
PLA	63	123	-	153	-	9.8	25.0	-
PLA/DL10	57	106	147	154	8.7	9.9	25.2	-
PLA/DL10/ZnO3	57	119	150	154	9.1	9.9	25.5	-
PLA/DL10/ZnO5	55	116	-	153	-	9.7	16.4	2
PLA/DL10/ZnO8	54	101	137	150	7.5	9.3	27.9	6
PLA/DL10/O-ZnO3	56	118	146	153	8.6	9.7	27.3	2
PLA/DL10/O-ZnO5	54	113	-	152	-	9.4	26.5	5
PLA/DL10/O-ZnO8	55	99	136	152	7.4	9.4	28.0	6
PLA/DL20	50	91	138	155	7.5	10.0	27.0	-
PLA/DL20/ZnO3	55	117	-	153	-	9.7	27.0	5
PLA/DL20/ZnO5	53	102	142	157	8.1	10.4	28.2	5
PLA/DL20/ZnO8	47	94	133	150	7.1	9.1	27.1	6
PLA/DL20/O-ZnO3	55	116	-	153	-	9.7	27.0	-
PLA/DL20/O-ZnO5	53	102	142	157	8.1	10.4	24.9	5
PLA/DL20/O-ZnO8	47	95	133	150	7.1	9.1	26.3	11

The D-limonene incorporation into the PLA promoted a decrease in the glass transition temperature (T_g) in comparison to the neat PLA. This effect was more prominent for the higher concentration of the D-limonene. These results are similar to those reported by other authors, where the D-limonene was used as plasticizer, leading to the increment of mobility of PLA chains and displacing the glass transition towards lower temperatures. [15,16,54] ~~Moreover, it must be highlighted that the obtained thermograms showed a single glass transition for the blend, corroborating the appropriate miscibility between D-limonene and PLA. [48]~~ In the nanocomposites, the glass transition temperature revealed an unclear tendency. On the one hand, for the nanocomposites with D-limonene (10 wt%), the T_g remained virtually unaltered compared to the blend. On the other hand, those with D-limonene (20 wt%), raw (ZnO), and modified (O-ZnO) (3 and 5 wt. %) nanoparticles, T_g increased slightly, except for higher concentration. The Tg of the PLA/ZnO showed the same behavior than PLA/O-ZnO. This behavior would suggest that nanoparticles with such high percentages may have agglomerated and did not alter the glass transition of the PLA matrix.

The incorporation of D-limonene decreased the cold crystallization temperature (T_{cc}) in comparison to pure PLA. As cited before, the plasticizers increased the PLA chain mobility and, therefore, the ability of PLA to crystalize. However, the use of nanoparticles slightly moved the cold crystallization towards higher temperatures, although they were lower than those of pure PLA. Therefore, the nucleating effect of the nanoparticles was demonstrated. These effects were more evident with higher percentages of plasticizer and nanoparticles. Other authors reported similar results with different plasticizers and fillers, which suggested a reduced crystallization induction period for the presence of crystalline nuclei and the enhanced nucleating behavior, respectively. [55–58]

The melting transition revealed changes due to the presence of D-limonene and nanoparticles. In general, multiple melting peaks appeared, ascribed to polymorphism of the crystalline structure.

Whereas, in some compositions, peaks and maximum temperatures could be identified (T_{m1} and T_{m2}). In some others, a shoulder was found, where it was not possible to identify the peak temperature. This shoulder-like behavior prevailed for the nanocomposites with D-limonene (10 wt%) and ZnO/O-ZnO (5 wt%), and those with D-limonene (20 wt%) and nanoparticles (3 wt%). The endothermic process at a lower temperature may be related to the melting of meso-stable crystals formed during cooling in the processing stage, as suggested by the lower calculated lamellar thickness (l_c). The second peak may correspond to more stable crystals with higher l_c that melted afterwards, explaining the high-temperature endothermic transition. Indeed, the maximum lamellar thickness was identified in nanocomposites with D-limonene (20 wt%) and ZnO and O-ZnO (5 wt%), around 10.4 nm. Although nucleating agents are known to generate multiple nuclei with a low lamellar thickness, the synergistic performance of D-limonene and nanoparticles in these percentages resulted in a semicrystalline structure with the highest degree of perfection. Complementarily, it has also been reported that the crystalline structures with lower lamellar thickness created during processing could also reorganize during heating, resulting in this multiple-peak melting behavior. [3,59]

The neat melting enthalpy, considered as the sum of melting and cold crystallization in the range from 70 to 180 ºC, is negligible for PLA and PLA with D-limonene, highlighting the amorphous structure of these materials. [42] However, the presence of ZnO and O-ZnO promoted a slight increase in the degree of crystallinity (X_c) compared to neat PLA, reaching values of up to 11%. The addition of ZnO and O-ZnO nanoparticles slightly increased the crystalline fraction of PLA, as they acted as heterogeneous nucleating agents. [16,18] Similar phenomena were observed in the literature dealing with nanocomposites, mainly processed by melt blending, in which nanoparticles increase the crystallinity of the matrix due to nucleation during cooling. [29,60–62]

3.4. Thermal stability

The effects of the nanoparticle incorporation on the thermal stability of PLA/D-limonene/ZnO and PLA/D-limonene/O-ZnO nanocomposites were analyzed by thermogravimetric analysis (TGA) under an inert atmosphere. For representative purposes, **Figure 6** shows the derivative TGA curves for neat PLA, PLA/D-limonene (10 wt%), and nanocomposites with ZnO and O-ZnO (3, 5, and 8 wt%). The results, in terms of the temperature, for the mass loss of 10% (T_{10}) and the peak obtained from the derivative TGA curve (T_{max}) are summarized in **Table 3**.

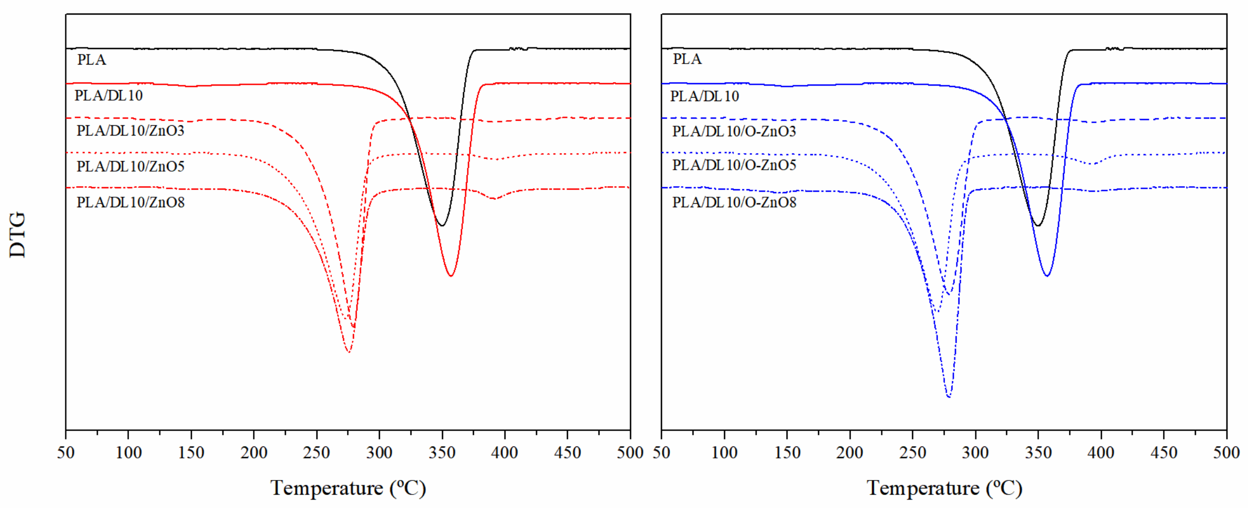

Figure 6. Derivative TGA thermograms of neat PLA, PLA/D-limonene, and nanocomposites with D-limonene (10 wt%, left; and 20 wt%, right).

The presence of D-limonene was discerned through a broad peak in the range between 125 and 200 ºC. [63] However, the peak revealed a non-significant contribution to the main thermal decomposition process, as shown by T_{10} values similar to those of pure PLA. However, T_{10} and T_{max} decreased due to the incorporation of ZnO by 33% and 31%, respectively. These results were consistent with the TGA profile obtained by other authors, where the decrease in the thermal stability were explained by the catalytic activity of ZnO, which leads to the thermal degradation of the polymer at lower temperatures. [31,64] It has been reported that zinc compounds can catalyze both the intermolecular transesterification reactions, reducing the molar mass of PLA due to the unzipping depolymerization, finally leading to selective lactic acid formation. [32] Moreover, it has also been reported that ZnO is capable of anchoring PLA end groups and water molecules in its structure. Indeed, the small peak found around 390 ºC has been reported as the loss of PLA molecules adsorbed on the surface of ZnO nanoparticles. [65] Therefore, ZnO can also locally catalyze the hydrolytic degradation of PLA, reducing the molar mass of the polymer and, consequently, its thermal stability. [65–67] In this regard, it is worth mentioning that given the sensitivity of PLA to temperature and hydrolysis, chain extenders can be added during processing to overcome these limitations, such as epoxy-functional styrene-acrylic oligomers or surface treatment of ZnO nanoparticles with specific silanes. [68]

Table 3. Results of thermal stability of PLA, PLA/D-limonene, PLA/D-limonene/ZnO, and PLA/D-limonene/O-ZnO nanocomposites. Standard deviation below 2% was omitted for the sake of clarity.

	T_{10} (ºC)	T_{max1} (ºC)	T_{max2} (ºC)
PLA	321	349	-
PLA/DL10	326	356	-
PLA/DL10/ZnO3	245	279	-
PLA/DL10/ZnO5	238	272	390
PLA/DL10/ZnO8	241	275	390
PLA/DL10/O-ZnO3	235	279	-
PLA/DL10/O-ZnO5	245	268	393
PLA/DL10/O-ZnO8	240	270	390

3.5. Mechanical properties

The mechanical properties were evaluated through microhardness analysis because the PLA and PLA nanocomposites showed great brittleness, difficulty the preparation of the typical specimens for the tensile test but the microhardness and the elastic modulus have been reported to be reciprocally dependent, and both are correlated to the polymer structure and composition. [59,69–71] The Vickers microhardness (*HV*) of the neat PLA, PLA/D-limonene, and nanocomposites were measured, and the obtained results are displayed in **Figure 7**.

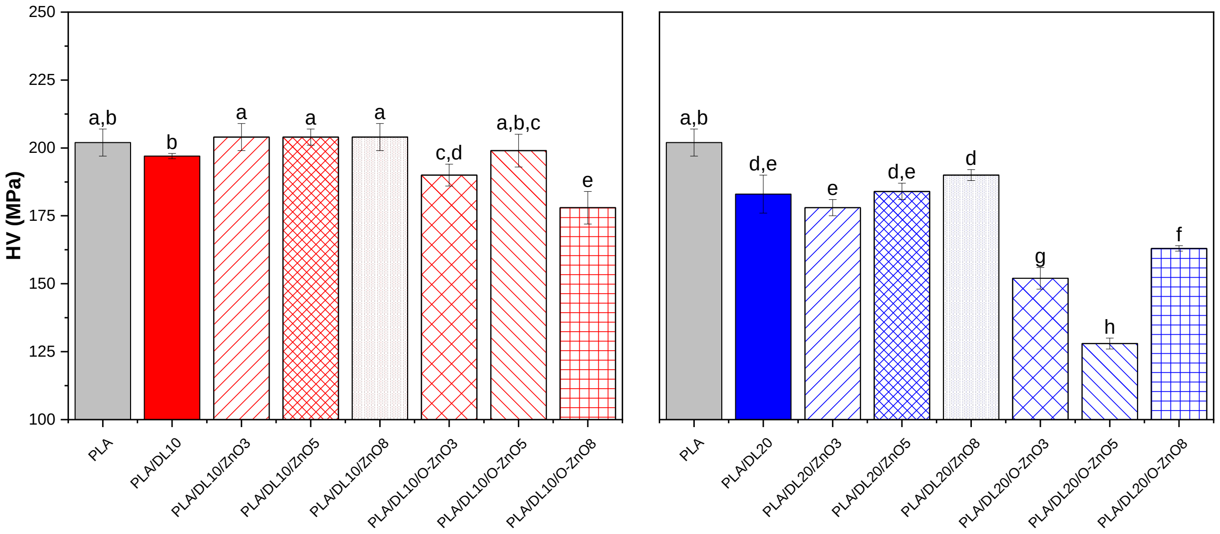

Figure 7. Vickers microhardness (*HV*) of neat PLA, PLA/D-limonene, and nanocomposites with D-limonene (10 wt%, left; and 20wt%, right). The same lowercase letters indicate that there is no significant difference (P>0.05).

Microhardness around 200 MPa was found for pure PLA, which decreased with the incorporation of D-limonene. This reduction was more relevant for the composition with D-limonene (20 wt%), which decreased by 9%, down to 183 MPa. ~~The microhardness and the elastic modulus have been reported to be reciprocally dependent, and both are correlated to the polymer structure and composition. [55,66,88]~~ In this regard, the use of plasticizers may lead to a decrease in the elastic modulus of PLA by reducing rigidity, allowing for the segmental mobility of macromolecular chains and, subsequently, for the plastic deformation of the amorphous fraction of PLA, which would reduce yield stress and increase elongation at break. [5,16]

Incorporating ZnO slightly increased the microhardness in the nanocomposites in comparison to both blends with D-limonene (10 and 20 wt%). The ZnO nanoparticles may bring rigidity to PLA, due to a uniform dispersion of the filler and positive interaction with the polymer matrix. [31,53,72,73] The increase in ZnO concentration may restrict PLA chain movement of, and, consequently, the elastic modulus would increase. [74] Moreover, the nucleating behavior of nanoparticles found in previous sections may result in more crystalline domains that impair the movement of the amorphous sections, resulting in higher rigidity. However, the presence of modified O-ZnO generally decreased the microhardness. Indeed, the lowest *HV* values in this study were found for nanocomposites involving O-ZnO and D-limonene (20 wt%). The contribution of the oleic acid to the surface of O-ZnO may have acted as a lubricant for the polymer matrix, counteracting the previously described contribution of the nanoparticles. [75,76]

3.6. Microbiological analysis

The antimicrobial properties against *E. coli* of the PLA/D-limonene and the nanocomposites with ZnO and O-ZnO (3, 5, and 8 wt%) were subsequently analyzed, and the obtained results are displayed in **Table 4**. The bacterial reduction was measured after UV light irradiation and compared after white light irradiation.

Table 4. Bacterial reduction percentage of *E. coli* by PLA/D-limonene, PLA/D-limonene/ZnO, and PLA/D-limonene/O-ZnO nanocomposites after UV and white light irradiation. Standard deviation was omitted for the sake of clarity

	Bacterial reduction (%)	
	UV light	**White light**
PLA/DL10	-	43.8
PLA/DL10/ZnO3	11.7	77.3
PLA/DL10/ZnO5	99.9	85.6
PLA/DL10/ZnO8	99.9	99.9
PLA/DL10/O-ZnO3	84.8	97.2
PLA/DL10/O-ZnO5	99.9	98.7
PLA/DL10/O-ZnO8	99.9	99.9
PLA/DL20	26.1	22.9
PLA/DL20/ZnO3	17.8	93.8
PLA/DL20/ZnO5	99.9	99.9
PLA/DL20/ZnO8	99.9	99.9
PLA/DL20/O-ZnO3	99.2	87.2
PLA/DL20/O-ZnO5	99.9	99.9
PLA/DL20/O-ZnO8	99.9	99.9

*The sign – indicates that bacterial reduction was not identified.

Bacterial reduction percentage by PLA/D-limonene with UV light was not identified but presented antimicrobial properties against *E. coli* up to 43.8% after white light irradiation. Previous studies demonstrated that D-limonene possesses antibacterial properties when exposed to air. [77] D-limonene has been reported to attack the cytoplasmic membranes of microorganisms, leading to the loss of the membrane integrity, dissipation of proton-motive forces, and the inhibition of respiratory enzymes. [78,79]

The antimicrobial properties of the composites with nanoparticle contents above 5 wt% were independent of the source of irradiation, D-limonene concentration, and surface modification of the nanoparticles. In general, the nanocomposites were highly effective against *E. coli*, reaching values of 99.9% due to the synergic effect of the ZnO/O-ZnO nanoparticles and the D-limonene.

Although the antimicrobial mechanism of ZnO nanoparticles is still unclear, the antimicrobial activity of these nanoparticles has been attributed to four different mechanisms: (*i*) formation of reactive oxygen species (ROS), (*ii*) release of zinc cations from the surface of nanoparticles, (*iii*) interaction between nanoparticles and microbial cells and (*iv*) permeation of nanoparticles (ZnO) into the cell membrane. [23,33]

In an aqueous solution under UV radiation, the ZnO nanoparticles have a phototoxic effect producing hydrogen peroxide (H_2O_2) and superoxide ions (O^{2-}). It has been reported that the H_2O_2 can penetrate the cells, causing their peroxidation and subsequent death. [26,80] This behavior was suggested by other authors after the incorporation of ZnO/vermiculite nanofiller in low-density polyethylene (LDPE). [81] Long-term antibacterial effect of the nanocomposites was found against bacteria *E. faecalis* for a ZnO proportion of 10 wt% after 96 h UV light exposure. Furthermore, ZnO hydrolysis may produce Zn^{2+}, which generates toxicity in the medium containing the microorganisms. [23]

ZnO nanoparticles with a zeta potential of +24 mV can further interact by electrostatic forces with the bacterial cell membranes (negative charge) due to the presence of remnant carboxylic groups. This strong interaction can lead to the loss of phospholipid bilayer integrity and leakage of intracellular components from the cell, ultimately leading to cell death. [30,82] Thus, once the integrity of the bilayer is lost, the small ZnO nanoparticles may penetrate through the bacterial membranes, increasing their antibacterial activity. The contact of ZnO nanoparticles with the cellular walls destroys the integrity of the bacterial cells. [83,84]

Some studies have revealed that the toxicity of ZnO nanoparticles occurs in dark conditions. [33,85] Therefore, it can be suggested that antimicrobial activity is not only affected by ROS production. The strong antimicrobial property of ZnO found in this study can only be explained by the synergistic contribution of all the proposed mechanisms together. It may occur that one mechanism prevails over the others; however, this is not yet fully understood. [33,85]

Similar studies in the literature found that the antibacterial activity against *E. coli* increased with ZnO incorporation and contact time. For instance, Marra et *al.* studied the reduction of *E. coli* in PLA/ZnO microcomposite films with ZnO (1, 3. and 5 wt%; 0.2-1.5 μm of diameter) [86] and Shankar *et al.* studied the incorporation of ZnO (0.5, 1.0, and 1.5 wt%; 56.1 nm of diameter) into PLA. [31] Therefore, it may be concluded that the toxicity of the ZnO nanoparticles against microorganisms may further depend on various factors such as the size of the particles, composition of growth media, and other physiochemical parameters. [87,88]

4. Conclusions

ZnO nanoparticles with 13.5 nm of diameter were successfully synthesized, modified with oleic acid (O-ZnO), and incorporated via melt compounding with PLA matrix using D-limonene as plasticizer.

The contribution of D-limonene (10 and 20 wt%) was demonstrated as plasticizer for the PLA matrix, as revealed by the glass transition temperature decrease ca. 9.5 and 20.6% in comparison with the pure PLA. The presence of O-ZnO in the PLA promoted a slight increase in the degree of crystallinity and acted as a driving force for the PLA to crystalize due to its nucleant performance. Thermal stability decreased with the incorporation of ZnO/O-ZnO. T_{max} of PLA decreased about 22.6% with the loading of ZnO/O-ZnO, due to catalytic activity of these nanoparticles that enhanced the PLA thermal degradation. Even so, the values are still suitable for the applicability of these materials.

The microhardness decreased with the incorporation of D-limonene, especially loading 20 wt% (ca. 9%) and incorporating the O-ZnO (ca. 31%), highlighting the D-limonene plasticizing effect and the feasible contribution of the oleic acid of the functionalized nanoparticles.

High efficiency of the antimicrobial performance against *E. coli* of the nanocomposites with nanoparticles concentration above 5 wt% of ZnO and O-ZnO was found regardless of irradiation source and D-limonene concentration.

Altogether, the nanocomposites with D-limonene (20 wt%) and O-ZnO (5 and 8 wt%) emerge as promising candidates with suitable thermal stability, higher ductility, and fully antimicrobial performance. These can be considered cost-effective and renewable alternatives in the packaging sector.

Acknowledgments

P.A. Zapata acknowledges the financial support under FONDECYT Regular Project 1170226. V.Moreno-Serna acknowledges the financial support under DICYT project 022041ZR_POSTDOCT. J.A. Ortiz thanks the financial support of ANID FONDECYT Postdoctorado 3200296. Generalitat Valenciana is acknowledged for the post-doctoral contract of O. Gil-Castell (APOSTD/2020/155).

Conflict of interest

The authors declare no conflict of interest.

References

1. De Silva, R. T.; Pasbakhsh, P.; Lee, S. M.; Kit, A. Y. *Appl. Clay Sci.* **2015**, *111*, 10.

2. Badia, J. D.; Gil-Castell, O.; Ribes-Greus, A. *Polym. Degrad. Stab.* **2017**, *137*, 35.

3. Fonseca, C.; Ochoa, A.; Ulloa, M. T.; Alvarez, E.; Canales, D.; Zapata, P. A. *Mater. Sci. Eng. C* **2015**, *57*, 314.

4. D'Amico, D. A.; Iglesias Montes, M. L.; Manfredi, L. B.; Cyras, V. P. *Polym. Test.* **2016**, *49*, 22.

5. Murariu, M.; Da Silva Ferreira, A.; Alexandre, M.; Dubois, P. *Polym. Adv. Technol.* **2008**, *19*, 636.

6. Pantani, R.; Gorrasi, G.; Vigliotta, G.; Murariu, M.; Dubois, P. *Eur. Polym. J.* **2013**, *49*, 3471.

7. Badia, J. D.; Gil-Castell, Ó.; Teruel-Juanes, R.; Ribes-Greus, A. *Ref. Modul. Mater. Sci. Mater. Eng.* **2019**.

8. Gil-Castell, O.; Andres-Puche, R.; Dominguez, E.; Verdejo, E.; Monreal, L.; Ribes-Greus, A. *Polym. Degrad. Stab.* **2020**, *180*, 109288.

9. Gil-Castell, O.; Badia, J. D.; Ingles-Mascaros, S.; Teruel-Juanes, R.; Serra, A.; Ribes-Greus, A. *Polym. Degrad. Stab.* **2018**, *158*, 40.

10. Cooper, J. A.; Lu, H. H.; Ko, F. K.; Freeman, J. W.; Laurencin, C. T. *Biomaterials* **2005**, *26*, 1523.

11. Murariu, M.; Dubois, P. *Adv. Drug Deliv. Rev.* **2016**, *107*, 17.

12. Menčík, P.; Přikryl, R.; Stehnová, I.; Melčová, V.; Kontárová, S.; Figalla, S.; Alexy, P.; Bočkaj, J. *Materials (Basel).* **2018**, *11*, 1.

13. Negro, V.; Mancini, G.; Ruggeri, B.; Fino, D. *Bioresour. Technol.* **2016**, *214*, 806.

14. Gil-Castell, O.; Badia, J. D.; Ribes-Greus, A. *J. Renew. Mater.* **2018**, *6*, 370.

15. Arrieta MP, López J, Ferra´ndiz S, P. M. *Polym. Test.* **2013**, *32*, 760.

16. Brüster, B.; Adjoua, Y. O.; Dieden, R.; Grysan, P.; Federico, C. E.; Berthé, V.; Addiego, F. *Polymers (Basel).* **2019**, *11*, 1363.

17. Aggarwal, K. K.; Khanuja, S. P. S.; Ahmad, A.; Santha Kumar, T. R.; Gupta, V. K.; Kumar, S. *Flavour Fragr. J.* **2002**, *17*, 59.

18. Li, W.; Li, L.; Cao, Y.; Lan, T.; Chen, H.; Qin, Y. *Nanomaterials* **2017**, *7*, 1.

19. Shameli, K.; Mansor Bin Ahmad; Majid Darroudi; Russly Abdul Rahman; Maryam Jokar; Wan Md. Zin Wan Yunis; Nor Azowa Ibrahim *Int. J. Nanomedicine* **2010**, *5*, 573.

20. Cai, S.; Pourdeyhimi, B.; Loboa, E. G. *ACS Appl. Mater. Interfaces* **2017**, *9*, 21105.

21. Cai, S.; Pourdeyhimi, B.; Loboa, E. G. *J. Biomed. Mater. Res. Part B Appl. Biomater.* **2019**, *107*, 900.

22. Yu, Z.; Wang, W.; Kong, F.; Lin, M.; Mustapha, A. *Int. J. Biol. Macromol.* **2019**, *129*, 887.

23. Rojas, K.; Canales, D.; Amigo, N.; Montoille, L.; Cament, A.; Rivas, L. M.; Gil-Castell, O.; Reyes, P.; Ulloa, M. T.; Ribes-Greus, A.; Zapata, P. A. *Compos. Part B Eng.* **2019**, *172*, 173.

24. Vasile, C.; Rapa, M.; Stefan, M.; Stan, M.; Macavei, S.; Darie-Nita, R. N.; Barbu-Tudoran, L.; Vodnar, D. C.; Popa, E. E.; Stefan, R.; Borodi, G.; Brebu, M. *Express Polym. Lett.* **2017**, *11*, 531.

25. Sirelkhatim, A.; Mahmud, S.; Seeni, A.; Kaus, N. H. M.; Ann, L. C.; Bakhori, S. K. M.; Hasan, H.; Mohamad, D. *Nano-Micro Lett.* **2015**, *7*, 219.

26. Padmavathy, N.; Vijayaraghavan, R. *Sci. Technol. Adv. Mater.* **2008**, *9*, 2.

27. Wong, S. W. Y.; Leung, P. T. Y.; Djurišić, A. B.; Leung, K. M. Y. *Anal. Bioanal. Chem.* **2009**, *396*, 609.

28. Wu, B.; Wang, Y.; Lee, Y. H.; Horst, A.; Wang, Z.; Chen, D. R.; Sureshkumar, R.; Tang, Y. J. *Environ. Sci. Technol.* **2010**, *44*, 1484.

29. Bussiere, P. O.; Therias, S.; Gardette, J.-L.; Murariu, M.; Dubois, P.; Baba, M. *Phys. Chem. Chem. Phys.* **2012**, *14*, 12301.

30. Fiedot-Toboła, M.; Ciesielska, M.; Maliszewska, I.; Rac-Rumijowska, O.; Suchorska-Woźniak, P.; Teterycz, H.; Bryjak, M. *Materials (Basel).* **2018**, *11*, 1.

31. Shankar, S.; Wang, L.-F.; Rhim, J.-W. *Mater. Sci. Eng. C* **2018**, *93*, 289.

32. Murariu, M.; Doumbia, A.; Bonnaud, L.; Dechief, A. L.; Paint, Y.; Ferreira, M.; Campagne, C.; Devaux, E.; Dubois, P. *Biomacromolecules* **2011**, *12*, 1762.

33. Zhang, H.; Hortal, M.; Jordá-Beneyto, M.; Rosa, E.; Lara-Lledo, M.; Lorente, I. *LWT* **2017**, *78*, 250.

34. Cifuentes, S. C.; Lieblich, M.; Saldaña, L.; González-Carrasco, J. L.; Benavente, R. *Materialia* **2019**, *6*, 100270.

35. Amigo, N., Palza, H., Canales, D., Sepúlveda, F., Vasco, D. A., Sepúlveda, F., & Zapata, P. A. *Compos. Part B Eng.* **2019**, *174*, 106979.

36. Bobillier, F.; Canales, D.; Antonella, F.; Cament, A.; Rivas, L. M.; Ulloa, T.; Reyes, P.; Ortiz, J. A.; Tatiana, G.; Loyo, C.; Zapata, P. A. *Polymers (Basel).* **2020**, *12*, 2132.

37. Zapata, P. A.; Palza, H.; Díaz, B.; Armijo, A.; Sepúlveda, F.; Ortiz, J. A.; Ramírez, M. P.; Oyarzún, C. *Molecules* **2019**, *24*, 1.

38. Canales, D.; Saavedra, M.; Flores, M. T.; Bejarano, J.; Ortiz, J. A.; Orihuela, P.; Alfaro, A.; Pabón, E.; Palza, H.; Zapata, P. A. *J. Biomed. Mater. Res. - Part A* **2020**, 2032.

39. Lauritzen, J. I.; Hoffman, J. D. *J. Chem. Phys.* **1959**, *31*, 1680.

40. Hoffman, J. D.; Lauritzen, J. I. *J. Res. Natl. Bur. Stand. - A. Phys. Chem.* **1961**, *65*, 1961.

41. Vasanthakumari, R.; Pennings, A. J. *Polymer (Guildf).* **1983**, *24*, 175.

42. Perez, E.; Perefia, J. M.; Benavente, R.; Bello, A.; Lorenzo, V. *Polym. Bull.* **1992**, *29*, 233.

43. ISO - ISO 20743:2013 - Textiles — Determination of antibacterial activity of textile products.

44. Wu, C.; Huang, Q. *J. Lumin.* **2010**, *130*, 2136.

45. Molefe, F. V; Koao, L. F.; Dejene, B. F.; Swart, H. C. *Opt. Mater. (Amst).* **2015**, *46*, 292.

46. Ortiz, J. A.; Catalina, F.; Corrales, T.; Soto, C.; Zapata, P. A. *Polym. Test.* **2020**, *81*.

47. Ortiz, J. A.; Matsuhiro, B.; Zapata, P. A.; Corrales, T.; Catalina, F. *Carbohydr. Polym.* **2018**, *182*, 81.
48. Smith, B. *Infrared Spectral Interpretation: A Systematic Approach*; Smith, B., Ed.; First edit.; CRC Press, **1998**.
49. Robinet, L.; Corbeil, M.-C. *Stud. Conserv.* **2003**, *48*, 23.
50. Li, Z.; Zhu, Y. *Appl. Surf. Sci.* **2003**, *211*, 315.
51. Arrieta, M. P.; López, J.; Hernández, A.; Rayón, E. *Eur. Polym. J.* **2014**, *50*, 255.
52. Yao, Y.; Ding, D.; Shao, H.; Peng, Q.; Huang, Y. *Int. J. Polym. Sci.* **2017**, *2017*, 1837171.
53. Cifuentes, S. C.; Frutos, E.; González-Carrasco, J. L.; Muñoz, M.; Multigner, M.; Chao, J.; Benavente, R.; Lieblich, M. *Mater. Lett.* **2012**, *74*, 239.
54. Abdelwahab, M. A.; Flynn, A.; Chiou, B. Sen; Imam, S.; Orts, W.; Chiellini, E. *Polym. Degrad. Stab.* **2012**, *97*, 1822.
55. Kulinski, Z.; Piorkowska, E. *Polymer (Guildf).* **2005**, *46*, 10290.
56. Xiao, H.; Lu, W.; Yeh, J.-T. *J. Appl. Polym. Sci.* **2009**, *113*, 112.
57. Yang, Z.; Peng, H.; Wang, W.; Liu, T.; Dobreva, T.; Benavente, R.; Pereña, J. M.; Pérez, E.; Avella, M.; García, M. *J. Appl. Polym. Sci.* **2010**, *116*, 1088.
58. Fukushima, K.; Tabuani, D.; Arena, M.; Gennari, M.; Camino, G. *React. Funct. Polym.* **2013**, *73*, 540.
59. Cifuentes, S. C.; Frutos, E.; Benavente, R.; Lorenzo, V.; González-Carrasco, J. L. *J. Mech. Behav. Biomed. Mater.* **2017**, *65*, 781.
60. Zhang, Y. C.; Xie, J. F.; Wu, H. Y.; Qiu, Y. P. *Mater. Sci. Forum* **2009**, *620–622*, 485.
61. Harris, A. M.; Lee, E. C. *J. Appl. Polym. Sci.* **2008**, *107*, 2246.
62. Ortenzi, M. A.; Basilissi, L.; Farina, H.; Di Silvestro, G.; Piergiovanni, L.; Mascheroni, E. *Eur. Polym. J.* **2015**, *66*, 478.
63. Andriotis, E. G.; Papi, R. M.; Paraskevopoulou, A.; Achilias, D. S. *Nanomaterials* **2021**, *11*, 1.
64. Virovska, D.; Paneva, D.; Manolova, N.; Rashkov, I.; Karashanova, D. *Appl. Surf. Sci.* **2014**, *311*, 842.
65. Qu, M.; Tu, H.; Amarante, M.; Song, Y.-Q.; Zhu, S. S. *J. Appl. Polym. Sci.* **2014**, *131*, 40287.
66. Nonato, R. C.; Mei, L. H. I.; Bonse, B. C.; Chinaglia, E. F.; Morales, A. R. *Eur. Polym. J.* **2019**, *114*, 271.
67. Lizundia, E.; Penayo, M. C.; Guinault, A.; Vilas, J. L.; Domenek, S. *Polym. Test.* **2019**, *75*, 175.
68. Murariu, M.; Paint, Y.; Murariu, O.; Raquez, J.-M.; Bonnaud, L.; Dubois, P. *J. Appl. Polym. Sci.* **2015**, *132*, 1.
69. Ostafinska, A.; Fortelný, I.; Hodan, J.; Krejčíková, S.; Nevoralová, M.; Kredatusová, J.; Kruliš, Z.; Kotek, J.; Šlouf, M. *J. Mech. Behav. Biomed. Mater.* **2017**, *69*, 229.

70. Tanase, C. E.; Spiridon, I. *Mater. Sci. Eng. C* **2014**, *40*, 242.

71. Montoille, L.; Morales, C.; Fontalba, D.; Ortiz, J. A.; Moreno-Serna, V.; Peponi, L.; Matiacevich, S.; Zapata, P. A. *Food Chem.* **2021**, *360*, 129966.

72. Panahandeh, N.; Torabzadeh, H.; Aghaee, M.; Hasani, E.; Safa, S. *J. Conserv. Dent.* **2018**, *21*, 130.

73. Ramezanzadeh, B.; Attar, M. M.; Farzam, M. *J. Therm. Anal. Calorim.* **2010**, *103*, 731.

74. Jayaramudu, J.; Das, K.; Sonakshi, M.; Siva Mohan Reddy, G.; Aderibigbe, B.; Sadiku, R.; Sinha Ray, S. *Int. J. Biol. Macromol.* **2014**, *64*, 428.

75. Ali, A. M. M.; Yahya, M. Z. A.; Mustaffa, M.; Ahmad, A. H.; Subban, R. H. Y.; Harun, M. K.; Mohamad, A. A. *Ionics (Kiel).* **2005**, *11*, 460.

76. Yahya, M. Z. A.; Arof, A. K. *Eur. Polym. J.* **2003**, *39*, 897.

77. Zukerman, I. *Nature* **1951**, *168*, 517.

78. Espina, L.; Gelaw, T. K.; de Lamo-Castellví, S.; Pagán, R.; García-Gonzalo, D. *PLoS One* **2013**, *8*, 1.

79. Zahi, M. R.; Liang, H.; Yuan, Q. *Food Control* **2015**, *50*, 554.

80. Lipovsky, A.; Nitzan, Y.; Gedanken, A.; Lubart, R. *Nanotechnology* **2011**, *22*, 1.

81. Čech Barabaszová, K.; Holešová, S.; Hundáková, M.; Pazdziora, E.; Ritz, M. *J. Inorg. Organomet. Polym. Mater.* **2017**, *27*, 986.

82. Zhang, L.; Ding, Y.; Povey, M.; York, D. *Prog. Nat. Sci.* **2008**, *18*, 939.

83. Zhang, L.; Jiang, Y.; Ding, Y.; Povey, M.; York, D. *J. Nanoparticle Res.* **2006**, *9*, 479.

84. Yang, H.; Liu, C.; Yang, D.; Zhang, H.; Xi, Z. *J. Appl. Toxicol.* **2009**, *29*, 69.

85. Shankar, S.; Teng, X.; Li, G.; Rhim, J. W. *Food Hydrocoll.* **2015**, *45*, 264.

86. Marra, A.; Silvestre, C.; Duraccio, D.; Cimmino, S. *Int. J. Biol. Macromol.* **2016**, *88*, 254.

87. Li, M.; Zhu, L.; Lin, D. *Environ. Sci. Technol.* **2011**, *45*, 1977.

88. Applerot, G.; Perkas, N.; Amirian, G.; Girshevitz, O.; Gedanken, A. *Appl. Surf. Sci.* **2009**, *256*, 3.

ANNEX – OPEN ACCESS POLICIES

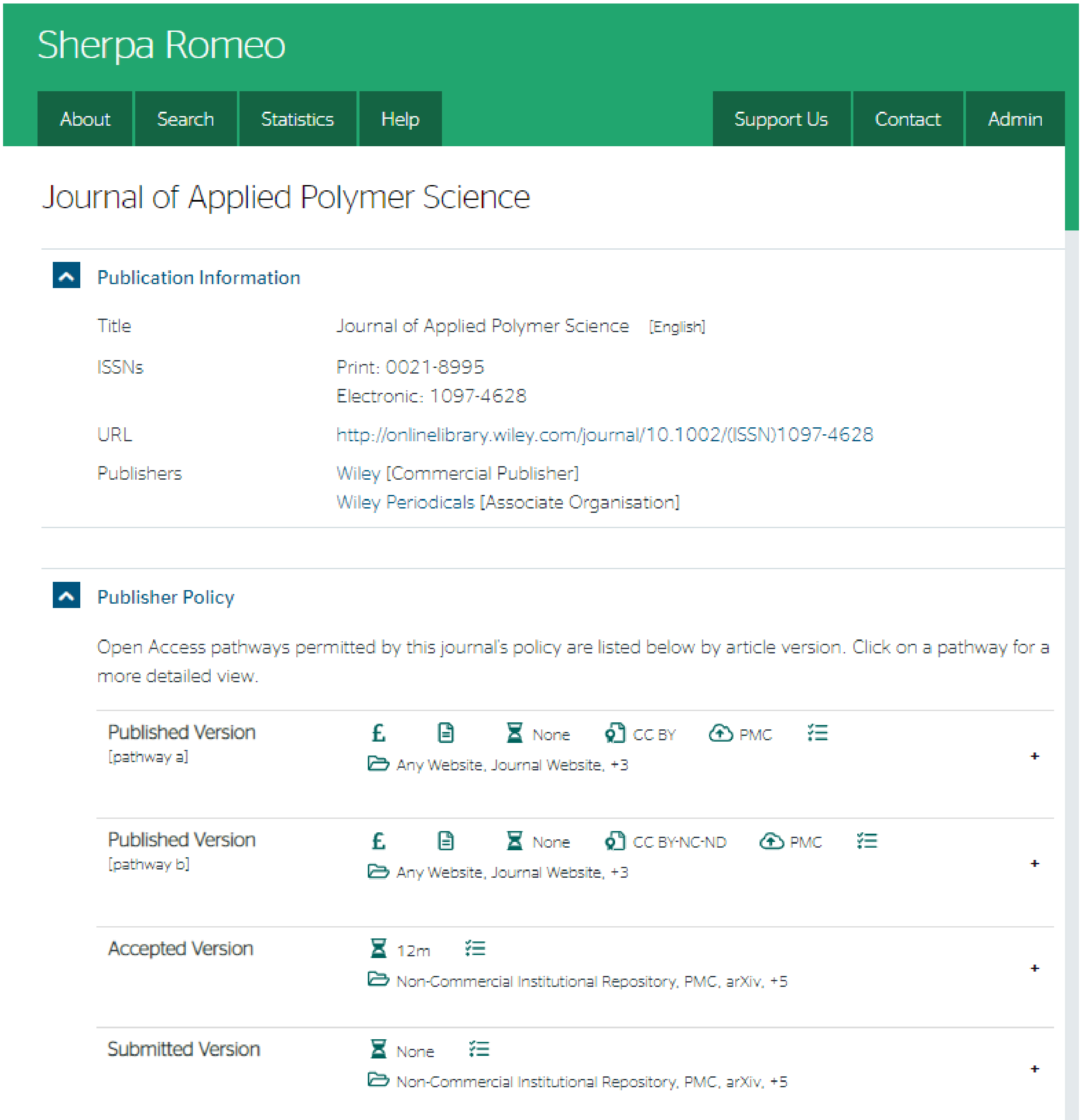

Journal of Applied Polymer Science

Publication Information

Title	Journal of Applied Polymer Science [English]
ISSNs	Print: 0021-8995 Electronic: 1097-4628
URL	http://onlinelibrary.wiley.com/journal/10.1002/(ISSN)1097-4628
Publishers	Wiley [Commercial Publisher] Wiley Periodicals [Associate Organisation]

Publisher Policy

Open Access pathways permitted by this journal's policy are listed below by article version. Click on a pathway for a more detailed view.

Published Version [pathway a]	£ None CC BY PMC Any Website, Journal Website, +3	+
Published Version [pathway b]	£ None CC BY-NC-ND PMC Any Website, Journal Website, +3	+
Accepted Version	12m Non-Commercial Institutional Repository, PMC, arXiv, +5	+
Submitted Version	None Non-Commercial Institutional Repository, PMC, arXiv, +5	+